JOURNAL OF GEOPHYSICAL RESEARCH, VOL. 92, NO. B10, PAGES 10,363-10,375, SEPTEMBER 10, 1987

PYRITE: SHOCK COMPRESSION, ISENTROPIC RELEASE, AND COMPOSITION OF THE EARTH'S CORE

Thomas J. Ahrens

Seismological Laboratory, California Institute of Technology, Pasadena

Raymond Jeanloz

Department of Geology and Geophysics, University of California, Berkeley

Abstract. New shock wave data (to 180 GPa) for pyrite (FeS_2) shocked along (001) demonstrate that this mineral, in contrast to other sulfides and oxides, does not undergo a major pressure-induced phase change over the entire pressure range (320 GPa) now explored. (This is probably so because of the initial, low-spin 3-d, orbital configuration of Fe^{+2}). The primary evidence which indicates that a large phase change does not occur is the approximate agreement of the shock velocity when extrapolated to zero particle velocity, 5.4 km/s, with the expected zero-pressure bulk sound speed of pyrite (5.36 to 5.43 km/s on the basis of previous ultrasonic data). Pyrite displays a prominent elastic shock (or Hugoniot elastic limit) of 8 ± 1 GPa. The velocity of the elastic shock approaches 8.72 km/s with decreasing shock pressure, the longitudinal elastic wave velocity. As shock pressure increases, the elastic shock velocity approaches 9.05 km/s and the elastic shock becomes overdriven for shock pressures greater than about 120 GPa. Analysis of release isentrope data obtained via the pressure-particle velocity buffer method indicates that buffer particle velocities in all experiments are from 1.7% to 20% greater than expected for a Grüneisen ratio given by 1.56 $(V/V_o)^{1.0}$. This discrepancy appears to result from volume increases upon pressure release of 0.04% to 4.5% which may result from shock-induced partial melting. The normalized pressure, finite-strain formalism for reducing Hugoniot data is extended to take into account initial porosity and shock-induced phase transitions. A least squares fit to the present and previous shock data for pyrite yields an isentropic bulk modulus, K_s, of 162 ± 9 GPa and a value of $dK_s/dP = 4.7 \pm 0.3$. This is close to the 145 ± 3 GPa bulk modulus observed ultrasonically. If the slight discrepancy in zero-pressure modulus is taken into account in the normalized pressure finite-strain formalism, a zero-pressure density of the shock-induced high-pressure phase having a density some 2% to 3% less than pyrite is inferred to occur in the high-pressure shocked state. We suggest from this result, the release isentrope results, and limited phase diagram data that the Hugoniot states probably correspond to material which is partially to completely melted. Using the above derived equation of state and previous shock wave data for iron, both the seismologically determined density and bulk modulus distribution in the outer core are fit to models with various temperature distributions and varying weight percent sulfur. Good agreement between the shock wave derived equation of state and the density/bulk modulus relations of the liquid outer core are obtained for temperatures of ~3000 K at the core/mantle boundary extending to 4400 K at the outer core-inner core boundary. For this thermal model a calculated sulfur content of $11 \pm 2\%$ is obtained.

Introduction and Background

The outer, liquid core of the earth extends from a radius of 1217 to 3486 km and represents some 31% of the earth's mass. Birch [1952] pointed out that the liquid core is some 10% less dense than that of pure liquid iron under the appropriate pressure and temperature conditions.

Paper number 6B6220.
0148-0227/87/006B-6220$05.00

Moreover, recent detailed analysis of shock wave and other thermodynamic data for iron by Jeanloz [1979] has demonstrated that the liquid core's bulk modulus is some 12% lower than that measured for pure iron. A number of authors have suggested that various possible cosmochemically abundant light elements are present in the earth's core. These include Si, C, and S [e.g., Ringwood, 1966, 1979; Jacobs, 1975]. These elements are depleted by various factors in the accessible crust and mantle of the earth [Murthy, 1976; Ringwood, 1979; Ahrens, 1979; Anderson, 1982; Brown et al., 1984] relative to carbonaceous chondritic and solar abundances. Moreover recently, experimental evidence that oxygen could be present in the earth's core stems from the enhanced solubility of O in liquid iron observed at high temperatures and pressures [Ohtani and Ringwood, 1984; Ohtani et al., 1984]. Also Fukai and Akimoto [1983] suggested that enhanced solubility of hydrogen may occur at high pressures in iron and that this element should also be considered as possibly alloying with iron in the outer core. Although it is possible that the light material in the core is actually a mixture of several elements rather than one element, as pointed out by both Ringwood [1979] and Stevenson [1981], on geochemical and dynamical grounds, respectively, it is important to recognize that exactly what the light element content of the core is, constrains the chemical environment which existed during the accretion of the earth with its present volatile budget. Volatiles affected by core formation include water [Lange and Ahrens, 1984; Hariya, 1984] and noble gases [e.g., Donahue and Pollack, 1983; Lewis and Prinn, 1984] as well as other species such as CH_4 and CO_2, important to man and the environment [Lange and Ahrens, 1986; Gold and Soter, 1980].

What different compositional models of the earth's core tell us about the accretion process and the total volatile budget has been studied to various degrees in the case of Si, O, H, and S. Briefly, Ringwood [1979] points out that if the earth accreted homogeneously, when it reached a radius in excess of 5000 km, selective volatilization of SiO would occur at surface temperatures above 1800 K, and some of the enstatite-rich chondritic material would react to form forsterite. Upon reduction of some of the SiO in the silicate to metallic silicon, this material could have been incorporated into a silicon-alloy iron core.

Ohtani et al. [1984] have shown that FeO will dissolve in liquid iron above ~2500-2900 K at atmospheric pressures, but such solution occurs at temperatures as low as 2500 K at 30 GPa. In contrast, incorporation of H into the core would appear to require very reducing surface conditions and inhibition of the iron-water surface reaction [Ringwood, 1979; Lange and Ahrens, 1984].

It has been argued that S cannot be the only light element in the core because then the earth would appear to be enriched and not depleted in S relative to similarly volatile elements in the earth's crust and upper mantle [Brown et al., 1984]. Because of the low eutectic temperature (1260 K) in the Fe-S system and the low shock pressure required to impact melt FeS (~33 GPa) [Anderson and Ahrens, 1986], an iron sulfide core would have started to form as the earth accreted and reached approximately 0.5 of its present radius. We note that the assumption that sulfur is the major light element alloying with iron in the core is supported by the recent work of Jones and Drake [1982] and Brett [1984], who find that the present siderophile minor element distribution of the earth's mantle is con-

TABLE 1. Hugoniot and Release

Shot Number	Impact Velocity, km/s	Impactor	Bulk Density, Mg/m^3	Archimedean Density, Mg/m^3	Elastic Shock Velocity, km/s	Final Shock Velocity, km/s	Final Particle Velocity, km/s	Shock Pressure, GPa	Shock Density, Mg/m^3
490	0.80	2024	4.9697	4.9931	8.743[a]	9.76	0.225[b]	9.76	5.100
	±0.02	Al	±0.0011	±0.0039	±0.113	±0.27	±0.007	±0.27	±0.005
509	1.337	2024	4.8541	4.916	8.826[c]	6.58	0.482	15.41	5.238
	±0.005	Al	±0.001	±0.003	±0.199	±0.17	±0.008	±0.20	±0.017
464	1.224	W	4.909	4.953	9.048	7.938	0.882	28.2	5.647
	±0.008		±0.011	±0.003	±0.037	±0.028	±0.007	±0.2	±0.013
472	1.578	W	4.908	4.961	8.999	7.034	1.133	39.13	5.850
	±0.003		±0.015	±0.005	±0.042	0.013	±0.006	±0.11	±0.013
483	2.499	W	4.903	4.944	8.971	7.938	1.771	68.94	6.311
	±0.014		±0.015	±0.003	±0.036	±0.028	0.012	±0.55	±0.019
505	2.532	W	4.794[d]	4.870	8.745	7.816	1.806	68.74	6.333
	±0.015		±0.001	±0.003	±0.033	±0.053	0.012	±0.55	±0.020
93LGG	4.866	2024	4.941	4.976	9.134	8.018	1.920	76.06	6.496
	±0.005	Al	±0.001	±0.004	±0.031	±0.046	±0.006	±0.24	±0.019
100LGG	5.733	2024	4.886	4.943	9.042	8.723	2.281	97.24	6.616
	±0.005	Al	±0.001	±0.003	±0.158	±0.062	±0.009	±0.35	±0.025
82LGG	6.233	2024	4.942	4.960	9.053	8.905	2.469	108.65	6.838
	±0.005	Al	±0.001	±0.004	±0.028	±0.008	±0.003	±0.119	±0.004
84LGG	5.478	Ta	4.916	4.958	[e]	10.321	3.586	181.94	7.534
	0.010		±0.001	±0.004		±0.094	±0.011	±1.24	±0.047

(a) Free surface velocity, elastic shock = 0.33 ± 0.17 km/s. Elastic shock amplitude (HEL) = 7.27 ± 1.52 GPa.
(b) Only elastic shock observed, final calculated state uses this velocity for impedance match solution.
(c) Free-surface velocity, elastic shock = 0.40 ± 0.013 km/s. HEL = 8.56 ± 0.19 GPa.
(d) Archimedean density used instead of bulk density for determination of shock state.
(e) Elastic shock overdriven.

sistent with that required for equilibrium with iron core material being formed at near-surface, but reducing, conditions in an accreting earth [e.g., Stevenson, 1981].

It has been argued for example in Ringwood [1979] (and discussed by Brown et al. [1984]) that if S were the major light element in the core, the upper mantle abundances of other nonsiderophile elements with similar or greater volatility than S are so low that the earth would, relative to these other elements (e.g., Sn, Zn, Se, Te, Ge, F, Ag, K, and Na), be enriched in S on account of 10% or 11% of the outer core being sulfur. This argument is sound. However, the mantle as a whole may be not as depleted in these volatile elements as our limited upper mantle sampling suggests. It should be pointed out that many of these elements concentrate in a component of the mantle which may have been produced when the protomantle was partially melted. The recent work of Rigden et al. [1984] prescribing the density of such basalticlike silicate compositions relative to mean upper mantle densities suggests that for partial melting in the mantle at pressures higher than 6 to 8 GPa, the resulting liquids will sink, not rise. Hence the mantle of the earth as a whole may have a larger inventory of some of the large ion lithophile elements and other volatile elements than an upper mantle sample which could be depleted in these elements may suggest. Both the possible existence of large ion lithophile elements and volatile enrichments in the lower mantle and the fact that partial melting upon impact accretion of FeS-rich compositions occurs early during earth accretion and core growth, make sulfur a likely element alloying with iron in the liquid outer core of the earth.

Previously [Ahrens, 1979; Brown et al., 1984] have studied dynamic compression of Fe_9S (pyrrhotite). Because pyrrhotite has a relatively low (0.39) mass fraction of sulfur relative to other minerals, it appears to be a good choice for studying the effect of a small amount of sulfur on the behavior of iron and is useful to place constraints on the sulfur content of the liquid outer core of the earth. In contrast, pyrite has a higher mass fraction of sulfur (0.53). However, as shown in the present study, and not appreciated previously, by Ahrens [1979] or in an earlier analysis by Batalov et al. [1976], this mineral does not undergo a major shock-induced phase change and thus removes a complication which unfortunately is imposed on the data analysis both in the case of iron and pyrrhotite. Although it is clear from the study of Brown and McQueen [1982] that the Hugoniot of iron represents the properties of the liquid above shock pressures of 250 GPa, the range in which either the Hugoniot of pyrite or pyrrhotite represents the liquid is uncertain. However, it should be pointed out because sulfur is simply a less important constituent in the core, the question of a liquid or solid Hugoniot is less critical in the case of the sulfide minerals.

Previously, Simakov et al. [1974] reported six Hugoniot data in the range from 28.9 to 320 GPa, which were independently analyzed in terms of hypothetical phase transitions by Batalov et al. [1976] and Ahrens [1979]. Previously, ultrasonic elastic constant data for pyrite are reported by several authors and collected by Simmons and Wang [1971]. In the present work some 10 new Hugoniot and release data extending to 180 GPa are presented, and a complete equation of state is derived. Both the Hugoniot elastic limit and the range of shock pressures in which a double shock wave exists are defined. We present new methods for reducing buffer-method release isentrope data to define release paths in the pressure-density plane and apply the reduced pressure/finite-strain formalism of Birch [1978] as specialized to shock data by Heinz and Jeanloz [1984] to infer (probably) partial melting in the shock state. Finally, the new data for pyrite are combined with existing shock wave data for iron and fit to the seismologically derived pressure/density/bulk moduli relations for the

Isentrope Data for Pyrite

Final State Free-Surface Velocity, km/s	Buffer Material	Buffer Shock Velocity, km/s	Release State Pressure, GPa	Release State Particle Velocity, km/s	Calculated Release State Particle Velocity, km/s	Calculated Release State Density, Mg/m^3	Calculated Excess Isentropic Release Volume, %
(b)	Lexan	2.69 ±0.01	0.61 ±0.03	0.191 ±0.008	(b)		
0.787 ±0.023	Lexan	2.78 ±0.01	1.42 ±0.03	0.427 ±0.008			
1.749 ±0.082	Lexan	4.965 ±0.025	9.87 ±0.15	1.667 ±0.016	1.373	5.234	4.5
2.47 ±0.22	Lexan	5.407 ±0.106	12.61 ±0.69	1.955 ±0.069	1.825	5.297	0.65
3.834 ±0.212	Lexan	6.894 ±0.045	24.41 ±0.41	2.968 ±0.030	2.760	5.543	0.92
	Lexan	6.831 ±0.180	23.8 ±1.6	2.926 ±0.120	2.769	5.530	0.53
	Fused Quartz	5.766 ±0.023	37.3 ±0.3	2.936 ±0.014	2.705	5.802	0.94
	Fused Quartz	6.436 ±0.014	47.6 ±0.2	3.358 ±0.009	3.226	5.960	0.24
	Fused Quartz	6.746 ±0.030	52.84 ±0.52	3.554 ±0.019	3.495	6.031	0.004
	Fused Quartz	9.220 ±0.045	103.89 ±1.08	5.113 ±0.028	4.665	6.642	1.4

earth. This results in constraints on the weight percent sulfur and to a lesser degree the temperature gradient, for a model liquid core assumed to be only a molten iron-sulfur liquid.

Experimental

Ten samples of natural pyrite from Ambasuguas, Spain, were machined into specimens 3 to 4 mm thick, flat and parallel to within ± 0.005 mm with lateral dimensions of 12 to 14 mm. Although the crystals were not specifically oriented, their well-defined crystal faces resulted in our propagating shocks within ±2° of the (001) direction.

Four microprobe analyses (A. Chodos, analyst) and reflection microscopy indicated only one phase was present in the samples. Three of the samples analyzed yielded data indicating a marginally detectable quantity of Ni, varying from 0.03 to 0.08 wt. % which was accounted for by assuming a pyrite-millerite (NiS) solid solution. Other elements for which we sought but did not find detectable concentrations (~ 0.1 wt. %) using X-ray dispersive analysis included Mg, Si, Ti, and Co. After taking into account the Ni content, the present samples appear to be still slightly more iron rich than FeS_2. Averaging the four analyses yielded the following solid solution representation of the sample material:

$$0.0715\ \text{FeS (troilite)} + 0.0008\ \text{NiS (millerite)} + \text{FeS}_2\ \text{(pyrite)} \quad (1)$$

The theoretical ideal solution density for this composition is 5.0002 Mg/m^3. This compares with 5.011 Mg/m^3 for pure pyrite. The theoretical value is close to the average of the Archimedean densities (Table 1) that were determined by measuring the mass of samples in air and toluene at carefully controlled temperatures. The average density is 4.947 ± 0.034 Mg/m^3. This Archimedean density value implies that our samples had an average inaccessible porosity of 1.08%. The average of nine bulk sample densities was 4.914 Mg/m^3, or 1.94% porosity. The latter value is close to the single value of bulk density, 4.91 Mg/m^3, reported by Simakov et al. [1974].

The samples after machining were mounted on 2024 Al, W, and Ta driver plates (Table 2). Metal flyer plate bearing projectiles were launched using the Caltech 40-mm propellant and 25-mm light gas guns [Ahrens, 1987]. The projectiles impacted the sample assemblies at speeds varying from 0.8 to 5.5 km/s (Table 1). Projectile velocity was determined by measuring laser interruption intervals [Ahrens et al., 1971] and via double exposure X-ray photography [Rigden et al., 1984] on the 40-mm apparatus and via X-ray shadowgraph on the light gas gun [Jeanloz and Ahrens, 1977]. All three systems employ time interval counter systems. Streak camera photography determined the elastic and deformational shock velocity and the free-surface velocity associated with the elastic and deformational shocks on the 40-mm and light gas gun apparatus [Vassiliou and Ahrens, 1982]. Isentropic release wave states were obtained upon reflection of the shock against 2-mm-thick lexan and fused quartz buffer samples on the 40-mm and light gas guns, respectively. The shock velocity is measured in the buffer material. From the known buffer equation of state, the pressure and particle velocity of the isentropically partially released state are determined [Ahrens and Rosenberg, 1968].

Results

Except for the highest pressure experiment (84LGG), double-shock structure was observed in all experiments. Although the initial shock velocity demonstrates some scatter, which can in part, be correlated with variations in

TABLE 2. Equation of State Standards

Material	ρ_o, Mg/m^3	C_o, km/s	S	Reference
2024 Al	2.785	5.328	1.338	McQueen et al. [1970]
W	19.224	4.029	1.237	McQueen et al. [1970]
Ta	16.678	3.293	1.307	Mitchell and Nellis [1981]
Lexan (<2.0 km/s)*	1.193	2.399	1.539	Marsh [1980]
(2.0-3.0 km/s)*	1.193	2.449	1.498	Marsh [1980]
Fused quartz	2.204	1.0861	1.599	Jackson and Ahrens [1979]

*Particle velocity.

initial bulk velocity, the initial shock velocity data when plotted versus final shock pressure demonstrate a consistent increase in velocity with final driving pressure. Because the velocity appears to extrapolate to approximately the value of the longitudinal elastic velocity along (001), 8.72 km/s (Figure 1) and the absence of indications from the Hugoniot release isentropes which suggest phase changes, we infer that this initial shock is an elastic shock. The apparent variation in shock velocity is presumably the result of the phenomenon of the elastic shock precursor decay (stress relaxation) described in iron and other metals, and semiconducting elements, oxides, and here for the first time, a sulfide [Ahrens and Duvall, 1966; Ahrens, 1966; Asay et al., 1972; McQueen et al., 1970; Grady, 1977]. Two shots (490 and 509) yielded inclined mirror free-surface velocity records which gave values of 8 ± 1 GPa for the Hugoniot elastic limit. The curve drawn through the elastic velocity data (Figure 1) and the shock velocity/particle velocity relation (Figure 2) indicates that the elastic shock will be overdriven at about 120 GPa. This is consistent with its absence only in shot 84LGG.

The shock velocity/particle velocity (U_s–u_p) relation is well satisfied by a straight line fit which extrapolates closely to the average value of the ultrasonically determined bulk sound speed, $Co = (K_{0s}/\rho_0)^{1/2}$. Simmons and Wang [1971] list values which vary from 5.36 to 5.43 km/s. Here K_{0s} is the isentropic bulk modulus and ρ_o is the single-crystal density. The r^2 value for the fit given in Figure 2 which omits the lower pressure datum of the present and Simakov et al. [1974] data set (13 points) is 0.997, whereas the slightly different fit used in the subsequent analysis included shot 509 gave an $r^2 = 0.994$ and parameters are given in Table 3 (14 points). Because of the good correlation of Co determined from Figure 2 and the ultrasonic value of Co, we infer no major phase change occurs in FeS_2 over the pressure range (to 320 GPa), which has been studied to date. This conclusion differs from those inferred by early analyses by Batalov et al. [1976] and Ahrens [1979], who considered only the earlier, sparser data set of Simakov et al. [1974]. Recently Jephcoat et al. [1983] also found no transition in pyrite to 40 GPa upon hydrostatic compression. Jackson and Ringwood [1981] correctly inferred only on the basis of ultrasonic and the Simakov et al. data that no phase change occurred in pyrite.

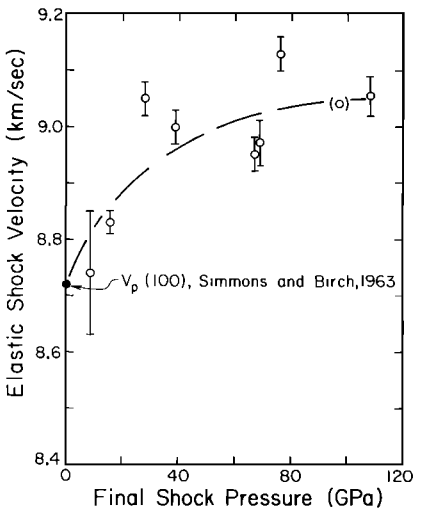

Fig. 1. Elastic shock velocity versus final shock pressure for pyrite, shocked along (001).

Since the above analysis of the U_s–u_p relation indicates no major phase changes upon shock compression, it is possible to use the STP value of the Grüneisen parameter, γ_o, to construct a complete equation of state. As indicated in Table 3, γ_o is calculated using a value of α, the thermal expansion coefficient of 13.7 x 10^{-5} K^{-1} [Skinner, 1966], K_{0s} of 147.9 GPa [Simmons and Birch, 1963], ρ_o and C_p of 5.016 Mg/m^3 and 0.518 kJ/kg/K [Robie et al., 1978]. These yield a value of 1.56 from the formula

$$\gamma_o = \alpha K_{0s}/C_p \rho_o \quad (2)$$

The particle velocity u_s achieved upon isentropic unloading from pressure, P_H, and particle velocity, u_H, to P_s, should for a known Grüneisen parameter, be exactly calculable from (Figures 3a and 3b)

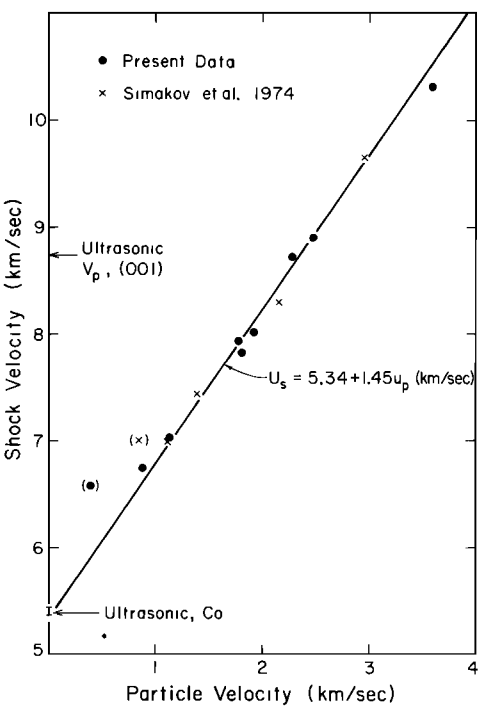

Fig. 2. Shock velocity versus particle velocity for pyrite. Data in parentheses not included in indicated fit (as elastic-deformational shock interaction may not have been properly taken into account).

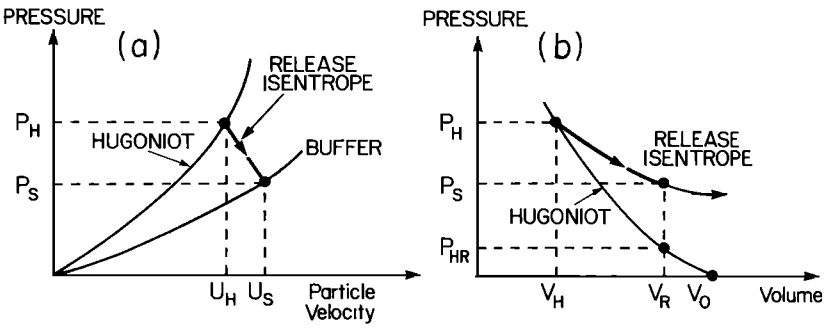

Fig. 3. Release isentrope (a) pressure-particle velocity and (b) pressure-volume relations. Equations (3) and (4) describe state along release isentrope indicated by heavy lines.

$$E_H - \int_{V_H}^{V_R} P_s\, dV = E_{HR} + (P_s - P_{HR})\, V/\gamma \qquad (3)$$

$$u_s = u_H + \left(\int_{V_H}^{V_R} P_s dV\right)^{1/2} \qquad (4)$$

where γ/V is assumed constant, and E_H and E_{HR} are the Hugoniot energy at states (P_H, V_H), and (P_{HR}, V_R), given by

$$E_H = P_H\,(V_o - V_H)/2 \qquad (5)$$

$$E_{HR} = P_{HR}\,(V_o - V_R)/2 \qquad (6)$$

Also P_s is the release pressure obtained at the buffer-sample interface upon reflection of a shock of amplitude P_H with particle velocity u_H. Equations (3)-(6) have been solved numerically to yield the release isentropes in both the pressure/particle velocity plane and pressure-volume plane along paths indicated by the heavy lines in Figures 3a and 3b. The pressure-density path for two of nine release isentropes is calculated using (3) and plotted in Figure 4. We note in Table 1 that in all cases the value of u_s, calculated using (3), with the assumption that γ_o=1.56 and γ/V is a constant is always (for all eight experiments where buffer data are available) slightly greater (by 1.7% to 21%) than those, u_r, measured. Several explanations of this discrepancy are possible. Two which have been considered are that the calculated value of γ_o (from (2)) used is too low. We find that values of $\gamma_o \sim 4$ are required to fit the theoretical values of u_s to u_r. Since the values of γ for minerals, compounds, and elements generally only range over the values of $\sim$1 to 2.5, we exclude this possibility. A more likely explanation is that partial or complete melting is occurring upon isentropic pressure release. The increase in volume, ΔVm, can be approximately calculated from the discrepancy between u_s and u_r using the equation [Lyzenga and Ahrens, 1978]

$$\Delta Vm \simeq 4(u_r - u_s)^2/(P_H + P_s) \qquad (7)$$

which yields approximate volume increases of 0.04% to 4.5% (Table 1) averaging 1.1% in eight experiments.

The Hugoniot pressure in terms of a Mie-Grüneisen equation of state is [e.g., Ahrens, 1979]

$$P_H = \left\{P_S + (\gamma/V)\left[\left(\int_{V_{02}}^{V} P_S dV\right) - E_{tr}\right]\right\} \times \left\{1 - (\gamma/V)\,(V_{oo} - V)/2\right\}^{-1} \qquad (8)$$

Here, sample porosity and phase transformations are accommodated: V_{00} is the initial sample volume (whether or not porous) and E_{tr} is the internal energy of transformation, with P_s and γ being the isentrope pressure and Grüneisen parameter at the Hugoniot volume. If the Hugoniot represents a high-pressure phase, V_{02} is its zero-pressure volume. Without a phase transformation, E_{tr} = 0, and V_{02} is the crystal volume of the starting material; if in addition there is no porosity, $V_{00} = V_{02}$.

As first pointed out by Jeanloz and Ahrens [1980], (8) can be expressed as a linear least squares problem in which the P_H (V) Hugoniot data are fitted to an Eulerian finite-strain form of the isentrope P_s(V). The justification for using the Eulerian finite-strain (Birch-Murnaghan) type of equation of state is that it is empirically known to be exceptionally successful in relating compression data to independently measured elastic moduli [e.g., Birch, 1978; Heinz and Jeanloz, 1984].

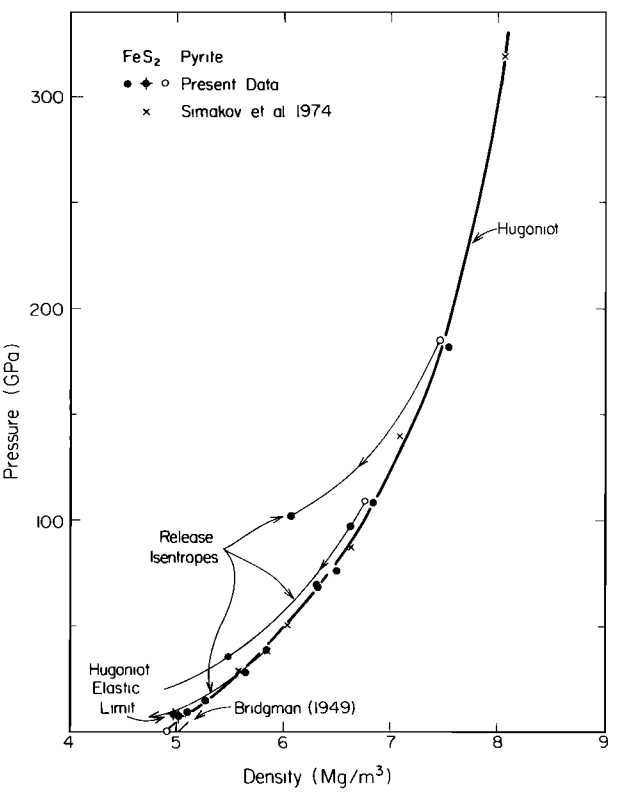

Fig. 4. Shock pressure versus density for pyrite. An analytic fit was used for calculating pressure-density isentropes; states (indicated by open circles) upon which isentropes are centered do not exactly coincide with Hugoniot data.

TABLE 3. Equations of

Material	Crystal Density, Mg/m^3	Bulk Density, Mg/m^3	C_o, km/s	S	S", $(km/s)^{-1}$	K_{os}, GPa
Pyrite	4.947[a]	4.914[b]	5.478[c]	1.401[c]		162[d] ±1.1
Iron	8.31[g]	7.85[h]	3.574[h]	1.92[h]	-0.068	0.068[h] ±0.7
Iron	8.31[g]	7.85[k]	3.80[k]	1.58[k]		140.0[l] ±3.2

(a) Measured average Archimedean density.
(b) Measured average bulk density.
(c) Fit to 14 data points (present data, plus Simikov et al. [1974]).
(d) Least squares fit to all but the three lowest data points taking into account individual initial bulk densities.
(e) First value least squares fit of (9) to average value of C for release isentropes, n = -0.6; second value, n = 1.0.
(f) First term 3R, second term after Brown et al. [1984].
(g) Jeanloz [1979].
(h) McQueen et al. [1970].
(i) Fit similar to that of (d), except for Hugoniot data between 40.9 and 319 GPa.
(j) Transition energy of melting [Brown et al., 1984].
(k) Al'tshuler et al. [1962].
(l) Fit similar to that of (k), except for Hugoniot data range from 35 to 315 GPa.

Thus the isentrope derived from the Hugoniot is expressed as a normalized pressure (F_{HS}) that is a polynomial expansion in terms dependent on the Eulerian strain:

$$f = \left[(V_o/V)^{2/3} - 1\right]/2 \quad (9)$$

Specifically [see Heinz and Jeanloz, 1984],

$$F'_{HS} = F_{HS} + \Delta F_{tr} = K_{0S}\,(1 - 2\xi_S\, f_{3H} + 4\varsigma_s\, f_{4H}^2 + ...) \quad (10)$$

with

$$F_{HS} = P_H \left[1-\gamma(R(2f+1)^{1.5}-1)/2\right] \Big/ \left\{ \left[1+(2-1.5\gamma)f\right] (3f)(1+2f)^{1.5} \right\} \quad (11)$$

where $R \equiv V_{oo}/V_o$.

$$\Delta F_{tr} = (E_{tr}/V_o)\,\gamma \left\{3f[1 + (2-1.5\,\gamma)f]\right\}^{-1} \quad (12)$$

$$f_{3H} = f[1+(2-\gamma)f]/[1 + (2-1.5\gamma)f] \quad (13)$$

$$f_{4H} = f\left\{[1+(2-0.75\gamma)f]/[1+(2-1.5\gamma)f]\right\}^{0.5} \quad (14)$$

Terms (11) - (14) are considered measured (or independently known), and these are used to determine the equation-of-state parameters for the phase represented by the Hugoniot: K_{0S} is the zero-pressure isentropic bulk modulus and

$$\xi = 3(4-K_0')/4 \quad (15)$$

$$\varsigma = (3/8)\left[K_0\, K_0'' + K_0'\,(K_0'-7) + 143/9\right] \quad (16)$$

are the third- and fourth-order terms in the finite-strain expansion [Birch, 1978]. Here K_0' is $(\partial K_{0S}/\partial P)_s$. Throughout these equations, subscripts zero and S indicate zero-pressure and isentropic conditions, respectively, and prime indicates differentiation with respect to pressure.

Equation (10) is analogous to Birch's F - f expression for compression data, but now modified to include the thermal correction to Hugoniot data. The normalized isentropic pressure, in contrast to (10) is

$$F = P_s[3f(1 + 2f)^{5/2}]^{-1} \quad (17)$$

which reflects the derivative of the equation of state, converging to K_{0S} as pressure goes to zero (f=0). The energy of transition is included in (10) and (12) as a perturbation term ΔF_{tr}, which is typically much smaller than F_{HS}. Except for the incorporation of porosity and phase transition effects, the present analysis is similar to the development in the work by Heinz and Jeanloz [1984]. The appendix gives expressions for the propagation of errors.

The present results and those of Simakov et al. [1974] for pyrite are shown as raw Hugoniot data (F, f: using Hugoniot density and pressure in (9) and (17): no symbols) and reduced points (F_{HS}, f_{3H}: open and solid symbols) in Figure 5. For the present purposes the approximation $f_{4H} \simeq f_{3H}$ is adequate, so the reduced values of normalized pressure F_{HS} are expected to follow a polynomial curve in the strain f_{3H}. To calculate the strain, the crystal density $\rho_0 = 1/V_o = 5.002\ Mg/m^3$ is used and the Grüneisen parameter is assumed to be given by Bassett et al. [1968].

$$\gamma = \gamma_0\,(V/V_0)^q \quad (18)$$

with uncertainties of $\gamma_0 = 1.56(\pm 0.16)$ and $q = 1.0\ (\pm 0.5)$. For each datum, the measured bulk density ρ_{00} (Table 1) is used to define the porous volume, and it is assumed that no phase transition occurs ($\Delta F_{tr} = 0$; K_{0S}, ξ_S, ς_S, and γ all pertain to the initial pyrite structure).

The present data and those of Simakov et al. are remarkably compatible, recognizing that an F - f plot such as Figure 5 tends to exaggerate scatter or discrepancies among compression measurements [Birch, 1978]. Although the present lowest pressure points fall well above the trend of the data in the figure, these deviations can be ascribed to the small (~ 1 - 2 %) initial porosities of the samples. That is, the porosity may not be fully overcome in the lowest pressure measurements. Similarly, the highest point of Simakov et al. exhibits a large value of F_{HS}. However, this cannot be plausibly explained by initial porosity. Instead, a slope or curvature in the F_{HS}–f_H trend (i.e., third- or higher-order terms in the equation of state), the effect of a phase transition (including melting), or large uncertainties in that measurement can all be offered as explanations for this last datum. Indeed, pyrite is likely to be molten along the Hugoniot at the pressures of the highest two or three points in Figure 3.

State, Pyrite and Iron

dK_{os}/dP	γ_o	n	E_{TR}, MJ/Mg	C_V, kJ/kg/K
4.7[d] ±0.3	1.56[e]	1.0		$0.624+0.080\times10^{-3}\ (V/V_o)T$[f]
5.28[i]	2.2[g]	1.62[g]	0.9[j]	$0.447+0.08\times10^{-3}(V/V_o)T$[f]
6.5[l]	2.2[g]	1.62[g]	0.9[j]	$0.447+0.08\times10^{-3}(V/V_o)T$[f]

A least squares fit to all but the three lowest points yields a zero-pressure bulk modulus of $K_{0S} = 162$ (±9) GPa ($K_{0S} = 4.7 \pm 0.3$). This is in relatively good accord with the ultrasonically determined $K_{0S} \simeq 145$ (±3) GPa for pyrite [Simmons and Wang, 1971], thus substantiating the point that no major phase transition occurs under shock loading. However, we note that the highest pressure datum of Simakov et al. biases the fit toward too low a bulk modulus. For example, the best fit to only the present data yields $K_{0S} = 174$ (±7) GPa (Figure 5). In this case, an equation of state of more than second order (Birch equation) is not statistically justifiable, so $K_{0S} = 4$, ξ_S=0 and $F_{SH} = 174$ is a constant with strain.

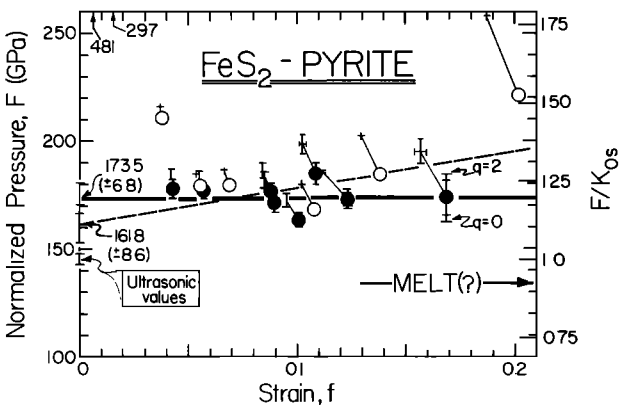

Fig. 5. Shock wave measurements on FeS_2 displayed in terms of normalized pressure F versus strain f. Reduced data (F_{HS}, f_{3H}) are shown by open [Simakov et al., 1974] and closed (present data) symbols which are tied to the raw Hugoniot points (F,f) shown as crosses and unadorned error bars. Two lowest present points lie off the plot at $F_{HS} = 481$ and 297 GPa. The larger error bars on F_{HS} (evident only at large strains) illustrate the additional uncertainty caused by letting q vary from 0 to 2. An unweighted fit to all but the three lowest points yields the dashed line ($K_{0S} = 161.8 \pm 8.6$ GPa), whereas a weighted fit to all but the two lowest present points yields the solid line ($K_{0S} = 173.5 \pm 6.8$ GPa, $K'_{0S} = 4$ assumed).

Regardless of how one fits the data, it is clear that the shock measurements systematically yield F_{SH} larger than the ultrasonic value of 145 GPa (Figure 5). The best fit to the present data results in a bulk modulus approximately 20% larger than the range of ultrasonic values, which is well outside the limits of estimated uncertainties. In addition, hydrostatic-compression measurements yield an isothermal value $K_{0T} = 143$ GPa that agrees with the ultrasonic measurements [Jephcoat and Olson, 1987]. Thus there is strong evidence that the Hugoniot data do not reflect the properties of the zero-pressure structure of pyrite, as determined by the ultrasonic and hydrostatic-compression experiments.

In order to better understand the nature of this discrepancy, it is worth examining the forms of (9) - (17) and the reduction of Hugoniot data in the F - f plane. In Figure 6 the thermal correction to the Hugoniot strain is illustrated for a range of γ encompassing the values that are encountered in practice. In all cases, the corrected strains f_{3H} and f_{4H} are larger than the raw (Hugoniot) value f, but the thermal correction is typically less than 20% up to a strain of 0.2. In particular, it is evident that for $\gamma \leq 1.5$ (high-pressure value), $f_{4H} \simeq f_{3H}$ to within 5% up to a strain $f = 0.2$. This justifies our current treatment of (10) as a polynomial expansion of F_{HS} in terms of f_{3H} alone, when considering the pyrite data. Clearly, there is no evidence for curvature in the F_{HS} reduced values in Figure 5 except possibly if one includes the highest pressure datum

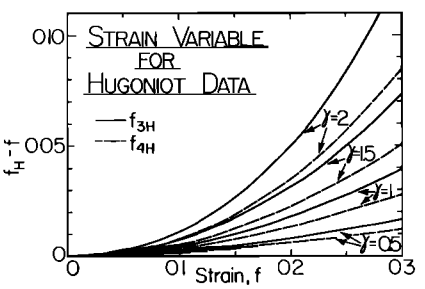

Fig. 6. Difference between the reduced strain f_H derived from (13) and (14) and the measured strain f from (9) is shown as a function of strain and Grüneisen parameter γ (taken to be constant for each curve).

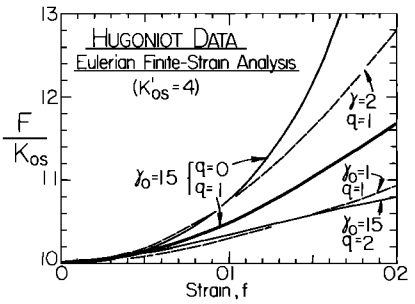

Fig. 7. Predicted Hugoniots shown as the nondimensional ratio F/K_{0S} versus strain f. The heavy curve is for a material described by a second-order ($K'_{0S} = 4$) Eulerian finite-strain equation of state with $\gamma_0 = 1.5$ and $q = 1$, and lighter (solid and dashed) curves illustrate the effects of varying γ_0 between 1 and 2 or q between 0 and 2 (see (18)). In all cases, the isentrope lies along the axis $F/K_{0S} = 1$.

of Simakov et al. As argued above, this point is perhaps best left out of the analysis. In either case, a linear (third-order) form of F_{HS} in f_{3H} is the most that is justified by the Hugoniot data. Ignoring the highest point, or considering only the present data, yields F_{HS} being statistically independent of f_{3H}, thus implying that a second-order equation of state is adequate (K_{0S}=4).

A second-order equation of state is given by $F_{HS}/K_{0S} = 1$. The relation of this isentrope to the raw Hugoniot is illustrated in Figure 7. Here, $\gamma_0 = 1.5$, $q = 1$ are taken as typical values, but the effect of varying γ_0 (1 to 2) and q (0 to 2) is also shown. For the parameters given, this figure summarizes how raw Hugoniot data (F versus f) would be reduced to the isentrope F_{HS}=K_{0S} = const when applying the thermal correction inherent in the Mie-Grüneisen formulation. For example, at a strain of 0.2 the normalized Hugoniot pressure F is corrected downward by 17% of K_{0S} ($\gamma_0 = 1.5$, $q = 1$, second-order equation of state). The uncertainties in the reduced values are therefore only a fraction of this 17% correction. Although these uncertainties increase with pressure (larger error bars with increasing strain in Figure 5), they remain small relative to the discrepancy between the Hugoniot-derived K_{0S} and ultrasonic bulk modulus for the pyrite data.

Up to this point, the effects of phase transitions have been ignored. The most important change due to a transition is in f, which in turn changes f_{3H}, F, and F_{HS} via (13), (17), and (11). By comparison, ΔF_{tr} gives only a small offset to F_{HS} in (10). This can be seen from characteristic values of $E_{tr}/V \sim 2$ GPa [e.g., Davies and Gaffney, 1973], which is of the order of 10^{-2} K_{02} for minerals. As the remaining terms in (12) amount to a factor of about 1 to 2, ΔF_{tr} is expected to change F_{HS} by only a few percent. Thus ΔF_{tr} can be safely ignored in the present discussion.

Assuming that the phase along the Hugoniot (indicated by subscript 2) is described by a second-order equation of state, F_2 = const independent of f_2. The observed strain is now given by

$$f = \left[(1 + 2 f_2)\left(V_{01}/V_{02}\right)^{2/3} - 1\right]/2 \qquad (19)$$

where the zero-pressure crystal volume of the initial phase is labelled by subscript 01 for clarity. Substituting (19) into (17) and (11) yields the observed normalized pressure including the phase transition. The resulting Hugoniots for volume ratios $0.95 \leq V_{01}/V_{02} \leq 1.05$ are summarized in Figure 8, which is an F - f plot showing the effects of a phase transition on the basic Hugoniot of Figure 7 (second-order adiabat, $\gamma_0 = 1.5$, $q = 1$, with $E_{tr} = \Delta F_{tr} = 0$).

What is clearly evident from Figure 8 is that a transition with a volume change of only a few percent can change the observed F by several tens of percent. For example, a volume change of 5% shifts the normalized pressure by about 40% at a strain of 0.1. In comparison, the thermal correction from Hugoniot to isentrope is only 5% at the same strain, and its uncertainty is likely to be much smaller (Figure 7). The change of F has the same sign as the volume change on transformation, and its magnitude increases drastically at small strains. That is, even a small increase in volume across a transition makes the equation of state appear anomalously stiff, and hence it significantly increases F at small strains.

Returning to Figure 5, it appears that the simplest interpretation of the reduced Hugoniot data (F_{HS} versus f_H) is that they reflect the properties of a different phase than the initial pyrite. That F_{HS} is systematically larger than the ultrasonic K_{0S} requires the new phase to be of larger volume (by up to ~2 or 3% from Figure 8) or to be less compressible (by up to F_{HS}/K_{0S} - 1 ~ 20%) than pyrite. The alternative possibility that ΔF_{tr} is responsible was shown above to be implausible: a strongly exothermic reaction ($E_{tr} < 0$) would increase F but only by a few percent, rather than ~ 20%.

Although there is a trade-off between contributions from changes in volume, bulk modulus, and internal energy, it seems that most if not all of the discrepancy between the F_{HS} values and the ultrasonic K_{0S} of pyrite can be accounted for by a small volume increase across a shock-induced transition. What is interesting is that such a transition could not be induced by pressure alone, because transformations caused by pressure must thermodynamically involve a volume decrease [e.g., Goodstein, 1975]. Therefore the temperature rise along the Hugoniot must be involved in creating what can be thought of as a high-temperature phase of FeS_2. Recognizing that pyrite melts incongruently at 1016 K at zero pressure [Kullerud, 1966], it is conceivable that partial or complete fusion explains the results of Figure 5.

The excess volume increases of up to ~4% observed upon isentropic release from pressures in the range 28 to 182 GPa suggest that the Hugoniot states are partially, rather than completely melted. Additional melting appears to take place upon isentropic release from this pressure range.

Application to the Earth's Core

Our tactic in this section is to construct an equation of state for molten iron and pyrite and compare these with the seismic models for the molten outer core.

The inner core is not treated here. Recently it has been modeled by Anderson [1986] and Jephcoat and Olson [1987], who conclude it is pure iron or contains a few percent of a light element, respectively.

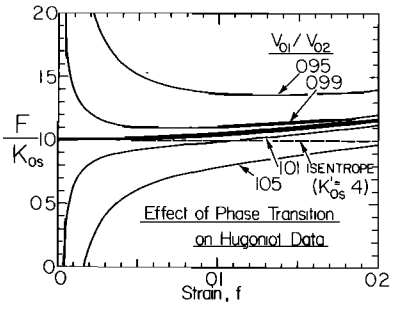

Fig. 8. Effect of a phase transition on the Hugoniot is displayed as nondimensional F/K_{0S} versus strain, for ratios of zero-pressure volume ranging between $V_{01}/V_{02} = 0.95$ and 1.05 (subscripts 1 and 2 refer to the initial sample and the phase achieved along the Hugoniot). In all cases, ΔF_{tr} in (10) is set to zero, and a second-order equation of state with $\gamma_0 = 1.5$, $q = 1$ is assumed. The bold curve is for $V_{01}/V_{02} = 1$, and it is identical to the bold curve in Figure 7; the corresponding isentrope is shown by the dashed line.

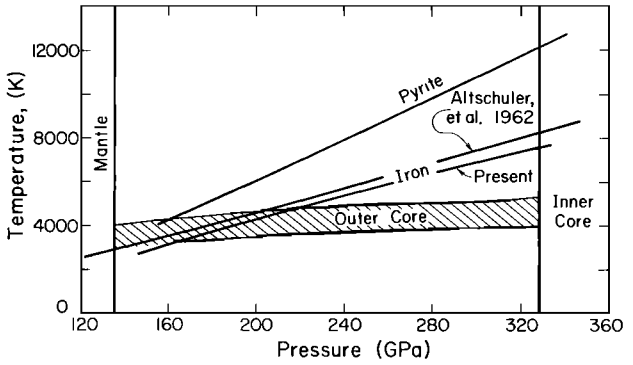

Fig. 9. Shock temperature versus shock pressure for pyrite and iron. Present calculation of shock temperatures for iron are shown for McQueen et al. [1970], and Brown and McQueen [1986] equation of state. Al'tshuler et al. [1962] shock temperatures are also shown.

Birch-Murnaghan parameters for iron over the pressure ranges indicated were obtained using both the McQueen et al. [1970] and Al'tshuler et al. [1962] shock wave data set (Table 3). It should be recognized that only in the case of iron are there definitive data [Brown and McQueen, 1986; Williams et al., 1987], which specify which portion of the high-pressure phase Hugoniot corresponds to the liquid (above ~250 GPa). The analysis of Jeanloz [1979] for the parameters γ_o and q, based on shock data for porous iron, however, most certainly reflect the properties of liquid. The trajectory of the iron Hugoniot in the pressure-temperature phase diagram has been recently discussed both by Brown and McQueen [1986] and Anderson [1986]. In order to estimate the shock pressures at which the pyrite Hugoniot is likely to go into the liquid field, we calculated shock temperatures from the formula [Ahrens, 1979]

$$T_s = 298 \exp\left[\gamma_o \rho_o^q (V_o^q - V^q)/q\right] \quad (20)$$

$$T_H = \{-3R + [9R^2 + 2\beta_o(V/V_o)(3RT_s + \beta_o(V/V_o)T_s^2/2 + (P_H - P_s)(V/\gamma))]^{1/2}\}/\left[\beta_o(V/V_o)\right] \quad (21)$$

where T_s is the temperature along the principal isentrope at volume V and T_H is the Hugoniot temperature. Equation (21) is derived for a material behaving with a specific heat which is the sum of lattice modes (3R) plus an electronic term $\beta_o (V/V_o)$ T as specified in Table 3. The resulting shock temperature calculations are shown for

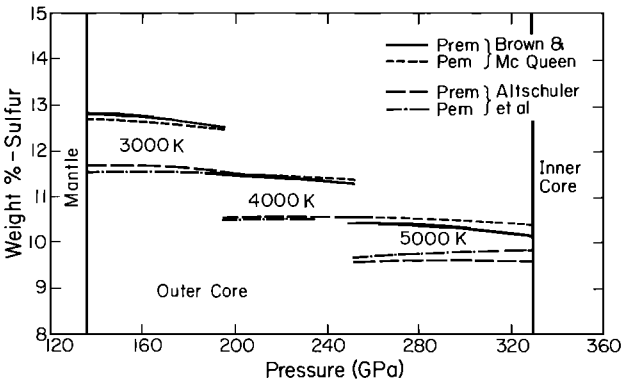

Fig. 10. Weight percent sulfur versus pressure for various isotherms and iron equations of state of McQueen et al. [1970], Brown and McQueen [1986], and Al'tshuler et al. [1962]. Curves are calculated for both PREM and PEM core models. Differences between two iron equations of state yield a difference of ~ 1% in apparent weight percent sulfur.

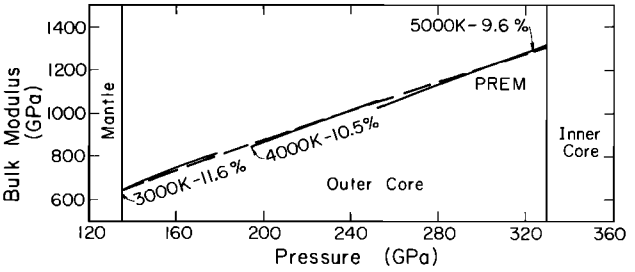

Fig. 11. Bulk modulus versus pressure in the outer core for 3000, 4000, and 5000 K isotherms constrained by PREM earth model. Average value of sulfur content in percent is indicated for each isotherm calculated with the Al'tshuler et al. [1962] iron equation of state.

pyrite and for the above equation-of-state formulation for iron in Figure 9. The latter calculation is comparable to that obtained by Al'tshuler et al. [1962] using a similar thermal formulation but a different equation of state. Since pyrite is more compressible, the calculated shock temperatures for pyrite are not unexpectedly substantially higher than iron. These values would be reduced perhaps by ~500 to 700 K if a fusion energy (unknown) were incorporated in the temperature calculation via E_{TR} in (8). We infer from both the excess volume upon release and the normalized volume fits of Figures 5 and 8 that the pyrite Hugoniot probably represents material in the liquid state over much of the pressure range of the outer core. We note that at zero pressure the FeS-FeS_2 eutectic (at 1356 K) occurs at substantially lower temperature than the iron melting point of 1812 K. Also since the iron Hugoniot crosses its fusion curve at 250 GPa, we might expect that pyrite will also be molten in this pressure range along the Hugoniot. The effect of the energy of melting on the present Hugoniot temperatures is such that they will be too high in the melt regime by ~550 ° C.

In order to calculate the mass fraction of sulfur which could account for the density deficit, relative to pure iron in the liquid outer core, specific volumes of iron, and FeS_2 at temperatures of 3000, 4000, and 5000K at a series of pressures corresponding to those of the outer core (135.8 to 328.9 GPa) were calculated from

$$(P_T - P_s)\frac{V}{\gamma} = 3R\,(T - T_s) + \frac{1}{2}\beta_o \frac{V}{V_o}(T^2 - T_s^2) \quad (22)$$

where P_s and T_s are given by (17) and (20). The independent variables for this calculation were the isothermal temperature, T, and P_T, the pressure at which the mass fraction S was to be calculated. The specific volume of each phase was then calculated by solving (22) via the Newton-Raphson method.

Since both the temperature and composition of the liquid core are unconstrained, we consider core composition in terms of three isotherms (Figure 10) in specific volume mixing calculations. The isotherms chosen, 3000, 4000, and 5000 K, are based on the thermal core models of Stacey [1977] and Stevenson [1981] and the application of (20). Using the Grüneisen parameters of iron for calculating the isentropic (adiabatic) temperature rise in the outer core yields values of 4010 K and 5346 K at the inner core boundary (ICB) starting with 3000 and 4000 K at the core mantle boundary (CMB). The steps in the density and bulk modulus curve (Figures 10-12) correspond to different isotherms. The core temperature, of course, varies smoothly with depth, rising some 1000 to 1500 K. Here we assume densities of 9.903 and 12.17 Mg/m^3 at the CMB and base of the outer core, respectively, from the preliminary reference earth model (PREM) of Dziewonski and Anderson [1981]. Calculating the specific volume of pyrite V_{pyr}, iron V_{Fe}, and the earth V_{ea}, using either the PREM or preliminary earth model PEM [Dziewonski et al., 1975] for V_{ea}, yields the mass fraction of pyrite at a given temperature as

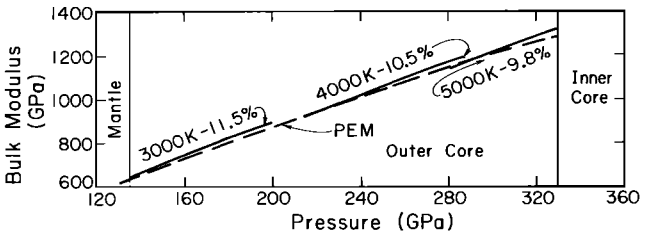

Fig. 12. Bulk modulus versus pressure for the outer core of the earth for isotherms at 3000, 4000, and 5000 K. PEM earth model was used. Percent sulfur shown is average for isotherm utilizing McQueen et al. [1970] and Brown and McQueen [1986] iron equation of state.

$$Y = (V_{ea} - V_{Fe}) / (V_{pyr} - V_{Fe}) \quad (23)$$

the mass fraction sulfur X is 0.534 Y. As can be seen in Figure 10, not only does the assumed temperature affect the calculated percent S in the outer core, but the differences between the Al'tshuler et al. [1962] and McQueen et al. [1970] equation of state of iron correspond to an equivalent of ~1000 K for each T. Notably the differences between the PREM and PEM affect the resultant mass fraction of S in only a minor way. Since we have not taken into account the heat of fusion, the isothermal volume of iron is slightly too small, as the thermal correction from the Hugoniot is too large. Therefore (23) gives a slight overestimate of S content in the core.

Ideally one might expect a nearly constant value of the weight percent with pressure if the outer core is, on the average, in a state of slight superadiabaticity and is convecting.

In order to further sort out the effect of temperatures, two models for the iron equations of state and slightly different earth models on the weight percent S, we have also examined the bulk modulus calculated for the percentage of sulfur which the above range of models predicts. Jeanloz [1979] pointed out the bulk modulus in the outer core was some ~12% lower than that of iron. The bulk modulus of a mixture of pyrite and liquid iron was then calculated using the Voigt-Reuss-Hill approximation [Watt et al., 1976]. Fitting the seismic data for the bulk modulus in the 3000 to 5000 K range using the PREM model, the Al'tshuler et al. iron equation of state and combined with the present pyrite equation of state yields the mass fractions, S, shown in Figure 11. The calculated percent S varies from 11.6% to 9.6% as the assumed temperature increases by ~2000 K from 3000 to 5000 K throughout the outer core. A fit which demands a more likely adiabatic temperature rise with depth in the core and a percentage S content, which is more nearly constant, can also be achieved by fitting simultaneously both the density and bulk moduli of the core with pressure, again using the Al'tshuler et al. equation of state for iron and the PEM model (Figure 12). The temperature rise with depth in the core inferred from this model is ~1400 K, whereas the variation of apparent S content with depth is from 11.5% to 9.8%. Both fits are close to the 10 (± 4)%S content inferred by Brown et al. [1984] on the basis of density using the high-pressure phase of pyrrhotite and iron equations of state at similar temperatures.

Discussion

An issue not yet addressed is the initial spin electronic states of FeS_2 (pyrite) versus pyrrhotite or troilite (FeS). Vaughan and Craig [1978] point out that in pyrite the 3-d, orbital electron configuration is initially in the low-spin state, whereas in $Fe_{1-x}S$ and FeS these start out with the high-spin configuration, and depending on details of the defect chemistry, the latter transform to phases with low-spin 3-d orbital configurations with increasing pressure. Thus both the phase changes in FeS and their absence in FeS_2 have some rationale.

Since the release isentrope experiments indicate a greater volume is achieved than can be readily explained with a plausible Grüneisen ratio, it appears that transition to a slightly lower density (~1%) phase is occurring upon pressure release. Also we observe the shock wave data fit the zero-pressure bulk moduli exactly in the F versus f analysis if a slight increase in apparent zero-pressure volume (2-3%) is assumed. If we associate both results, it may be that the shock wave data indicate that shock-induced melting is occurring (F-f, results), whereas upon unloading, additional pressure-release melting takes place. Further research on the high-pressure, high-temperature phase diagram of Fe_2S should clarify the situation.

With regard to application of the present results to constraining the possible sulfur content of the earth's outer liquid core, we have found that the shock wave data for pyrite probably represent the properties of the liquid. In the case of iron, the case for the shock data representing the properties of the liquid above 250 GPa is very strong (as inferred from sound speed and temperature shock measurements [Brown and McQueen, 1986; Williams et al., 1987]).

When the present data for pyrite are used in conjunction with iron data to fit the seismically derived pressure-density and pressure/bulk modulus profile of the outer core, several conclusions may be drawn.

1. Good agreement between the shock wave equation of state and the seismic data is obtained for temperatures of ~ 3000 K at the core-mantle boundary extending to 4400 K at the outer core/inner core boundary. For this thermal model a calculated sulfur content of 11 ± 2% is obtained in agreement with the results inferred by Anderson [1977], Ahrens [1979], and Brown et al. [1984].

2. Thermal and composition models of the outer core derived here are consistent with adiabatic variation of temperatures through the core by ~1500 K. However, the level of temperatures within the range ~3000-5000K are at least ~1500K lower than the ~6600 ± 500 K inferred by Williams et al. [1987] at the outer core/inner core boundary. This discrepancy could imply a much greater melting point depression than previously thought, which cannot be ruled out.

3. The conclusions concerning sulfur content change little using different core seismic models. However, the difference between the Brown and McQueen [1986] and Al'tshuler et al. [1962] data for iron translates into about a 1% difference in apparent sulfur content. Also of concern is the consistent apparent decrease by 2 1/2% in equivalent weight percent sulfur, in going from the core-mantle boundary to inner core/outer core boundary found in all combinations of seismic and equation-of-state models. Although such a compositional variation is not physically impossible, it may represent presently unrecognized inaccuracies in present Earth and material models.

Appendix: Uncertainties in Normalized Shock Pressure Finite-Strain Analysis

The following quantites are assumed to be either experimentally measured or estimated, and hence each can be assigned a standard deviation(s): P_H, V, V_o, V_{oo}, γ, q, E_{TR}. For purposes of error analysis we assume that the dependent variable defined in terms of the quantities in (10) is

$$F'_{HS} = F_{HS} + \Delta F_{tr} \quad (A1)$$

Paralleling the treatment in Heinz and Jeanloz [1984], we write, dropping the subscripts,

$$s^2(F')^2 = \left[\frac{\partial F'}{\partial f}\right]^2 s^2(f) + \left[\frac{\partial F'}{\partial \gamma}\right]^2 s^2(\gamma) + \left[\frac{\partial F'}{\partial P_H}\right]^2 s^2(P_H) + \left[\frac{\partial F'}{\partial E_{tr}}\right]^2 s^2(E_{tr}) + \left[\frac{\partial F'}{\partial V_o}\right]^2 s^2(V_o) + \left[\frac{\partial F'}{\partial V_{oo}}\right]^2 s^2(V_{oo}) \quad (A2)$$

where if we consider the first term in (A2), it in turn is the sum of two terms

$$\frac{\partial F'}{\partial f} = \frac{\partial F_{HS}}{\partial f} + \frac{\partial \Delta F}{\partial f} \quad \text{(A3)}$$

where the first term is

$$\frac{1}{P_H}\frac{\partial F}{\partial f} = -R\gamma/\{2f\,(1+2f)\,[1+(2-1.5\gamma)f]\}^{-1}$$

$$-\left\{[1-0.5\gamma(2f+1)^{3/2}\,R+0.5\gamma]\left\{(1+2f)^{-1}[3f+(6-4.5\gamma)f^2]\right.\right.$$

$$\left.\left.+[1+(4-3\gamma)f]\right\}\right\}/\left\{3f^2(1+2f)^{3/2}\left\{1+(2-1.5\gamma)f\right\}^2\right\} \quad \text{(A4)}$$

and the second is

$$\frac{\partial\,\Delta F}{\partial f} = -E_{TR}\gamma\,[3f[1+(2-1.5\gamma)f]]^{-2}(3+12f-9\gamma f)/V_o \quad \text{(A5)}$$

Since

$$s^2(f) = \left[\frac{\partial f}{\partial V}\right]^2 s^2(v) + \left[\frac{\partial f}{\partial V_o}\right]^2 s^2(V_o) \quad \text{(A6)}$$

we write

$$\frac{\partial f}{\partial V} = -(V_o/V)^{5/3}/(3V_o) \quad \text{(A7)}$$

$$\frac{\partial f}{\partial V_o} = (V_o/V)^{2/3}/(3V_o) \quad \text{(A8)}$$

The coefficient of the first term of (A2) can now be calculated using (A3)-(A8). The coefficient of the second term of (A2) is also given by two terms:

$$\frac{\partial F'}{\partial \gamma} = \frac{\partial F_{HS}}{\partial \gamma} + \frac{\partial \Delta F}{\partial \gamma} \quad \text{(A9)}$$

$$\frac{1}{P_H}\frac{\partial F}{\partial \gamma} = \left\{[1+(2-1.5\gamma)f][-0.5(2f+1)^{3/2}R+0.5]\right.$$

$$\left.+(1.5)(1-0.5\gamma(2f+1)^{3/2}\,R+0.5\gamma)f\right\}/$$

$$\left\{3f(1+2f)^{3/2}[1+(2-1.5\gamma)f]^2\right\} \quad \text{(A10)}$$

and

$$\frac{\partial \Delta F}{\partial \gamma} = E_{TR}\,[3V_o f[1+(2-1.5\gamma)f]]^{-1}$$

$$+ E_{TR}\,\gamma/\{2V_o[1+(2-1.5\gamma)f]^2\} \quad \text{(A11)}$$

The coefficient of the third term of (A2) is given by

$$\frac{\partial F'}{\partial P_H} = \frac{\partial F_{HS}}{\partial P_H} + \frac{\partial \Delta F}{\partial P_H} = \frac{F_{HS}}{P_H} \quad \text{(A12)}$$

The coefficient of the fourth term of (A2) is given by

$$\frac{\partial F'}{\partial E_{TR}} = \frac{\partial F_{HS}}{\partial E_{TR}} + \frac{\partial \Delta F}{\partial E_{TR}} = \frac{\Delta F}{E_{TR}} \quad \text{(A13)}$$

The coefficient of the fifth term of (A2) is given by

$$\frac{\partial F'}{\partial V_o} = 0.5\,P_H\gamma(2f+1)^{3/2}V_\infty/\left\{V_o^2[1+(2-1.5\gamma)f]3f(1+2f)^{3/2}\right\}$$

$$-E_{TR}\gamma[3V_o^2 f\,[1+(2-1.5\gamma)f]]^{-1} \quad \text{(A14)}$$

Finally the coefficient of the sixth term of (A2) is given by

$$\frac{\partial F'}{\partial V_\infty} = -P_H\gamma(2f+1)^{3/2}/\left\{6V_o f[1+(2-1.5\gamma)f]\right.$$

$$\left.(1+2f)^{3/2}\right\} \quad \text{(A15)}$$

The uncertainties in the independent variable of (10), f_{3H}, are specified by

$$s^2(f_{3H}) = \left[\frac{\partial f_{3H}}{\partial f}\right]^2 s^2(f) + \left[\frac{\partial f_{3H}}{\partial \gamma}\right]^2 s^2(\gamma) \quad \text{(A16)}$$

where

$$\frac{\partial f_{3H}}{\partial f} = \frac{1+f(4-2\gamma)}{1+2f-1.5\gamma f} - \frac{f[1+(2-\gamma)f](2-1.5\gamma)}{(1+2f-1.5\gamma f)^2} \quad \text{(A17)}$$

and

$$\frac{\partial f_{3H}}{\partial \gamma} = \frac{1.5f^2(1+(2-\gamma)f)-f^2(1+2f-1.5\gamma f)}{(1+2f-1.5\gamma f)^2} \quad \text{(A18)}$$

The $s^2(f)$ term in (A16) is specified by (A6)-(A8). Also

$$s^2(\gamma) = (V/V_o)^{2q}s^2(\gamma_o) + (q\,\gamma_o/V)^2(V/V_o)^{2q}\,s^2(V)$$

$$+(\gamma_o\,q/V_o)^2(V/V_o)^{2q}s^2(V_o)$$

$$+\,[\gamma\,ln\,(V/V_o)]^2\,s^2(q) \quad \text{(A19)}$$

Acknowledgments. Thomas J. Ahrens appreciates greatly the experimental assistance of C. Creaven, E. Gelle, and M. Long, and has profitted from technical discussions with D. Stevenson and G. Rossman, and the critical comments of two anonymous reviewers and of D. L. Anderson, M. Brown, and P. Watt on an earlier version of the manuscript. We thank A. P. Jephcoat for showing us his unpublished data. Supported under NSF grant EAR8219435. Division of Geological and Planetary Sciences, California Institute of Technology, contribution 4172.

References

Ahrens, T. J., High-pressure electrical behavior and equation of state of magnesium oxide from shock wave measurements, J. Appl. Phys., 37, 2532-2541, 1966.

Ahrens, T. J., Equations of state of iron sulfide and constraints on the sulfur content of the earth, J. Geophys. Res., 84, 985-998, 1979.

Ahrens, T. J., Shock wave techniques for geophysics and planetary physics, in Methods of Experimental Physics., edited by C. G. Sammis and T. L. Henyey, Academic, New York, in press, 1987.

Ahrens, T. J., and G. E. Duvall, Stress relaxation behind elastic shock waves in rock, J. Geophys. Res., 71, 4349-4360, 1966.

Ahrens, T. J., and J. T. Rosenberg, Shock metamorphism: Experiments on quartz and plagioclase, in Shock Metamorphism of Natural Materials, edited by B. M. French and N. M. Short, pp. 59-81, Mono Book, Baltimore, Md, 1968.

Ahrens, T. J., J. H. Lower, and P. L. Lagus, Equation of state of forsterite, J. Geophys. Res., 76, 518-528, 1971.

Al'tshuler, L. V., A. A. Bakanova, and R. F. Trunin, Shock adiabats and zero isotherms of seven metals at high pressures, Sov. Phys., JETP, Engl. Transl., 15, 65-74, 1962.

Anderson, D. L., Composition of the mantle and core, Ann. Rev. Earth Planet. Sci., 5, 179-202, 1977.

Anderson, O. L., The earth's core and the phase diagram of iron, Philos. Trans. R. Soc. London, Ser. A, 306, 21-35, 1982.

Anderson, O. L., Properties of iron at the Earth's core conditions, Geophys. J. R. Astron. Soc., 84, 561-579, 1986.

Anderson, W. W., and T. J. Ahrens, Shock wave experiments on iron sulfide and sulfur in planetary cores (abstract), Lunar Planet. Sci., XVII, 11-12, 1986.

Asay, J. R., G. R. Fowles, G. E. Duvall, M. H. Miles, and R. F. Tinder, Effect of point defects on elastic decay in LiF, J. Appl. Phys., 43, 2132-2145, 1972.

Bassett, W. A., T. Takahashi, H. K. Mao, and J. S. Weaver, Pressure-induced phase transformation in NaCl, J. Appl. Phys., 39, 319-325, 1968.

Batalov, V. A., V. A. Buzayeva, G. S. Telegin, and R. F. Trunin, Equations of state of metastable phase for twelve minerals, Izv. Earth Phys., 8, 530-534, 1976.

Birch, F., Elasticity and constitution of the earth's interior, J. Geophys. Res., 57, 227-286, 1952.
Birch, F., Finite strain isotherm and velocities for single-crystal and polycrystalline NaCl at high pressures and 300K, J. Geophys. Res., 83, 1257-1268, 1978.
Brett, R., Chemical equilibration of the earth's core and upper mantle, Geochim. Cosmochim. Acta, 48, 1183-1188, 1984.
Bridgman, P. W., Linear compressions to 30,000 kg/cm^2, including relatively incompressible substances, Proc. Am. Acad. Arts Sci., 77, 187-234, 1949.
Brown, J. M., and R. G. McQueen, The equation of state for iron and the earth's core, in High Pressure Research in Geophysics, edited by S. Akimoto and M. H. Manghnani, pp. 611-624, Center for Academic Publications, Tokyo, 1982.
Brown, J. M., and R. G. McQueen, Phase transitions, Grüneisen parameter, and elasticity for shocked iron between 77 GPa and 400 GPa, J. Geophys. Res., 91, 7485-7494, 1986.
Brown, J. M., T. J. Ahrens, and D. L. Shampine, Hugoniot data for pyrrhotite and the earth's core, J. Geophys. Res., 89, 6041-6048, 1984.
Davies, G. F., and E. S. Gaffney, Identification of high-pressure phases of rocks and minerals from Hugoniot data, Geophys. J. R. Astron. Soc., 33, 165-183, 1973.
Donahue, T. M., and J. B. Pollack, Origin and evolution of the atmosphere of Venus, in Venus, edited by D. M. Hunter, L. Colin, T. M. Donahue, and V. I. Moroz, pp. 1003-1036, University of Arizona Press, Tucson, 1983.
Dziewonski, A. M., D. L. Anderson, Preliminary reference earth model, Phys. Earth Planet. Inter., 25, 297-356, 1981.
Dziewonski, A. M., A. L. Hales, and E. R. Lapwood, Parametrically simple earth models consistent with geophysical data, Phys. Earth Planet. Inter., 10, 12-48, 1975.
Fukai, Y., and S. Akimoto, Hydrogen in the earth's core: Experimental approach, Proc. Jpn. Acad., 59B, 158-162, 1983.
Gold, T., and S. Soter, The deep-earth-gas hypothesis, Sci. Am., 154-161, June 1980.
Goodstein, D. L., States of Matter, 500 pp., Prentice-Hall, Englewood Cliffs, N. J., 1975.
Grady, D. E., Processes occurring in shock wave compression of rocks and minerals, in High Pressure Research: Applications in Geophysics, edited by M. H. Manghnani and S. Akimoto, pp. 389-438, Academic, New York, 1977.
Hariya, Y., H_2O in the earth's interior, in Material Science of the Earth's Interior, edited by I. Sunagawa, pp. 463-476, Terra Scientific Publishers, Tokyo, 1984.
Heinz, D. L., and R. Jeanloz, The equation of state of the gold calibration standard, J. Appl. Phys., 55, 885-893, 1984.
Jackson, I., and T J. Ahrens, Shock wave compression of single-crystal forsterite, J. Geophys. Res., 84, 3039-3048, 1979.
Jackson, I., and A. E. Ringwood, High pressure polymorphism of the iron oxides, Geophys. J. R. Astron. Soc., 67, 767-784, 1981.
Jacobs, J. A., The Earth's Core, 253 pp., Academic, New York, 1975.
Jeanloz, R., Properties of iron at high pressures and the state of the core, J. Geophys. Res., 84, 6059-6069, 1979.
Jeanloz, R., and T. J. Ahrens, Pyroxenes and olivines: Structural implications of shock-wave data for high pressure phases, in High-Pressure Research, edited by M. Manghnani and S. Akimoto, pp. 439-461, Academic, New York, 1977.
Jeanloz, R., and T. J. Ahrens, Equations of state of FeO and CaO, Geophys. J. R. Astron. Soc., 62, 505-528, 1980.
Jephcoat, A. P., and P. Olson, Is the inner core of the Earth pure iron? Nature, 325, 332-335, 1987.
Jephcoat, A. P., H. K. Mao, and P. M. Bell, Pyrite: Hydrostatic compression to 40 GPa, Eos Trans. AGU, 64, 847, 1983.
Jones, J. H., and M. J. Drake, An experimental approach to early planetary differentiation, Lunar Planet. Sci., XIII, 369-370, 1982.
Kullerud, G., Phase relations in sulfide-type systems, in Handbook of Physical Constants, Mem., 97, edited by S. P. Clarke, Jr., pp. 323-344, Geological Society of America, Boulder, Colo., 1966.
Lange, M. A., and T. J. Ahrens, FeO and H_2O and the homogeneous accretion of the earth, Earth Planet. Sci. Lett., 71, 111-119, 1984.
Lange, M. A., and T. J. Ahrens, Shock-induced CO_2 loss from $CaCO_3$: Implications for early planetary atmospheres, Earth Planet. Sci. Lett., 77, pp. 409-418, Elsevier Science Publishers B.V., 1986.
Lewis, J. S., and R. G. Prinn, Planets and Their Atmospheres, Origin and Evolution, 470 pp., Academic, New York, 1984.
Lyzenga, G., and T. J. Ahrens, The relations between the shock-induced free-surface velocity and post-shock density of solids, J. Appl. Phys., 49, 201-204, 1978.
Marsh, S. P. (Ed.), LASL Shock Hugoniot Data, 327 pp., University of California Press, Berkeley, 1980.
McQueen, R. G., S. P. Marsh, J. W. Taylor, J. N. Fritz, and W. J. Carter, The equation of state of solids from shock wave studies, in High Velocity Impact Phenomena, edited by R. Kinslow, pp. 294-419, Academic, New York, 1970.
Mitchell, A. C., and W. J. Nellis, Shock compression of aluminum, copper and tantalum, J. Appl. Phys., 52, 3363-3374, 1981.
Murthy, V. R., Composition of the core and the early chemical history of the earth, in The Early History of the Earth, edited by B. F. Windley, pp. 21-31, John Wiley, New York, 1976.
Ohtani, E., and A. E. Ringwood, Composition of the core, I., Solubility of oxygen in molten iron at high temperatures, Earth Planet. Sci. Lett., 71, 85-93, 1984.
Ohtani, E., A. E. Ringwood, and W. Hibberson, Composition of the core, II, Effect of high pressure on solubility of FeO in molten iron, Earth Planet. Sci. Lett., 71, 94-103, 1984.
Rigden, S. M., T. J. Ahrens, and E. M. Stolper, Densities of liquid silicates at high pressures, Science, 226, 1071-1074, 1984.
Ringwood, A. E., The chemical composition and origin of the earth, in Advances in Earth Science, edited by P. M. Hurley, pp. 287-356, MIT Press, Cambridge, Mass., 1966.
Ringwood, A. E., Origin of the Earth and the Moon, 295 pp., Springer-Verlag, New York, 1979.
Robie, R. A., B. S. Hemingway, and J. R. Fisher, Thermodynamic properties of minerals and related substances at 298.15K and 1 Bar (10^5 Pascals) pressure and at higher temperatures, U. S. Geol. Surv. Bull., 1452, 298-310, 1978.
Simakov, G. V., M. N. Pavlovskiy, N. G. Kalashnikov, and R. F. Trunin, Shock compressibility of twelve minerals, Izv. Phys. Solid Earth, 488-492, 1974.
Simmons, G., and F. Birch, Elastic constants of pyrite, J. Appl. Phys., 34, 2736-2738, 1963.
Simmons, G., and H. Wang, Single Crystal Elastic Constants and Calculated Aggregate Properties: A Handbook 2nd ed., 370 pp., MIT Press, Cambridge, Mass., 1971.
Skinner, B. J., Thermal expansion, in Handbook of Physical Constants, Mem. 97, edited by S. P. Clark, Jr., pp. 75-96, Geological Society of America, Boulder, Colo., 1966.
Stacey, F. D., Physics of the Earth, 2nd ed., 414 pp., John Wiley, New York, 1977.
Stevenson, D. J., Models of the earth's core, Science, 214, 611-619, 1981.
Vassiliou, M. S., and T. J. Ahrens, Limited aperture light source streak photography, Rev. Sci. Instrum., 53 (1), 108-109, 1982.

Vaughan, D. J., and J. R. Craig, Mineral Chemistry of Metal Sulfides, 493 pp., Cambridge University Press, New York, 1978.

Watt, J. P., G. F. Davies, and R. J. O'Connell, The elastic properties of composite materials, Rev. Geophys. 14, 541-563, 1976.

Williams, Q., R. Jeanloz, J. Bass, B. Svendsen, and T. J. Ahrens, The melting curve of iron to 250 Gigapascals: A constraint on the temperature at Earth's center, Science, 236, 181-182, 1987.

T. J. Ahrens, Seismological Laboratory 252-21, California Institute of Technology, Pasadena, CA 91125.

R. Jeanloz, Department of Geology and Geophysics, University of California, Berkeley, CA 94720.

(Received July 30, 1986;
revised June 5, 1987;
accepted June 9, 1987.)